Journal of Fluorescence
https://doi.org/10.1007/s10895-024-03584-1

RESEARCH

Synthesis of SiO_2@Ag Nanocomposite for Investigating Metal-Enhanced Fluorescence and Surface-Enhanced Raman Spectroscopy

Dang Van Thai[1,2] · Van Ben Pham[3] · Cong Doanh Sai[3] · Thi Huong Giang Nguyen[3] · Trong Duc Tran[3] · Thi Ha Tran[4] · Tien-Thanh Nguyen[5] · Tien Dai Nguyen[1,6] · Hong Van Bui[3]

Received: 24 November 2023 / Accepted: 9 January 2024

Abstract
SiO_2@Ag nanocomposite (NC) has been synthesized by the chemical reduction and Stöber method for Metal-enhanced fluorescence (MEF) of Rhodmine 6G (R6G) and Surface-enhanced Raman spectroscopy (SERS) of Malachite green (MG). As-synthesized SiO_2@Ag NC indicated SiO_2 nanosphere (NS) and Ag nanoparticle (NP) morphologies. The SiO_2@Ag NC was high quality with a well-defined crystallite phase with average sizes of 24 nm and 132 nm for Ag NP and SiO_2 NC, respectively. By using SiO_2@Ag NC, the photoluminescence (PL) intensity of the R6G (at 59.17 ppm) was increased approximately 133 times. The SERS of the MG (at 1.0 ppm) with SiO_2@Ag NC as substrate clearly observed vibrational modes in MG dye at 798, 916, 1172, 1394, and 1616 cm^{-1}. As a result, the SERS enhancement factor (EF_{SERS}) at 1172 cm^{-1} obtained 6.3×10^6. This initial study points to the potential of SiO_2@Ag NC as a promising material for MEF and SERS substrates to detect dyes at low concentrations.

Keywords SiO_2@Ag · Nanocomposite · Rhodamine 6G · SERS · Malachite green · Enhancement factor

Introduction

Nowadays, SiO_2-combined Ag NPs have been widely applied in bio-medicine [1, 2], aesthetics [3], optoelectronics [4, 5], pharmaceutical medicine [6], food technology [7, 8], early diagnosis [9], disease treatment [10], and environmental treatment [11–13]. The SiO_2 ingredient possesses thermal-stable, chemical-inert, and non-toxic properties. In addition, the SiO_2 nanostructure has been easily prepared in nanoparticle form and dispersed evenly in various solutions. Due to the high biocompatibility and functionalized surface, SiO_2 NPs can easily bond with pigments, metal ions, and biomolecules [11]. While Ag NPs- the rest of the NCs possess the surface plasmon resonance (SPR) peak at about 400 nm can produce SERS and MEF signals larger than that of metals with the absorption peak at visible or near-infrared regions [11, 14]. In the electromagnetic field of the incident light, the gap positions between Ag NPs are also known as hot spots, so the local electromagnetic field has been enhanced [11, 14, 15]. The intensity of the electromagnetic field gradually decreases from the center of the hot spots away.

SiO_2@Ag NC structures have been successfully prepared using different methods, which can control the morphology and size of SiO_2@Ag NCs, thereby affecting the MEF and SERS capabilities [16–20]. For example, SiO_2@Ag nanostructures were synthesized by sol–gel method with the decorated Ag NPs size of 35 nm on nano-sized SiO_2 spheres of 20–60 nm [16]. The co-precipitation process combined with polymerization created Ag@SiO_2 NCs

✉ Hong Van Bui
buihongvan@hus.edu.vn

1 Institute of Theoretical and Applied Research, Duy Tan University, Hanoi 100000, Vietnam

2 Faculty of Environmental and Chemical Engineering, Duy Tan University, Da Nang 550000, Vietnam

3 VNU University of Science, Vietnam National University - Hanoi, Hanoi 100000, Vietnam

4 Hanoi University of Mining and Geology, 18 Pho Vien, Bac Tu Liem, Hanoi, Vietnam

5 Institute of Materials Science, Vietnam Academy of Science and Technology, 18 Hoang Quoc Viet, Hanoi, Vietnam

6 Faculty of Natural Sciences, Duy Tan University, Da Nang 550000, Vietnam

Published online: 27 January 2024

with the spherical Ag core size in the order of micrometers within the SiO_2 shell [17]. Using the Stöber method, synthesized Ag@SiO_2 nanospheres had 80 nm sized Ag NPs on 800 nm sized SiO_2 spheres [21], core–shell Ag@SiO_2 NCs were composed of 50 nm sized Ag cores and 75 nm sized SiO_2 shells [22].

R6G is an organic dye widely used in industrial products for daily life. However, the release of the R6G dye into the environment will cause pollution and affect human health. R6G molecules always tend to form dimers or monomers. A charged redistribution in the molecules changes their fluorescent property [23–26]. PL spectrum often appears as a wide band with a peak position in the range of 550–630 nm, which is the superposition of some bands [27]. PL intensity and maximum position depend on the R6G concentration in the solution. At low concentrations, R6G molecules are not agglomerated into big clusters, so PL is characterized by monomers, while at more significant concentrations, it is dominated by dimers [23]. In the electromagnetic field of incident radiation, R6G molecules at the hot spots between Ag NPs receive substantial PL enhancement because of the MEF effect [28, 29]. Several studies have also shown that MEF occurs for R6G [28, 29] and other organic compounds [22]. Through supporting Ag nanoparticles, the MEF enhancement factor (EF_{MEF}) can be increased many times [30–35].

Besides, MG dye is also studied in this study. It is popular in the dye industry and aquaculture. The MG dye can be recognized at dilute concentration via the SERS [36]. For our initial studies, MG has been used as a probe to check whether a material could be used in SERS. The SERS of the MG appears clearly with characteristic peaks for vibration of binding groups in the molecular, and the intensity depends on the interaction between MG and metal NCs. The characteristic peaks of ring C–H in-plane bending and ring C–C stretching vibrations are usually very obvious and are chosen to calculate the enhancement factor [37, 38]. Enhancement factor determination allows it to appreciate the enhancement level of the SERS signal. Raman signals at low concentrations can reach approximately 10^5–10^8 thanks to the SERS of Ag NPs [37, 39–42]. In fact, the SERS is used as a tool to detect the concentration of dye compounds in inspection samples. Another concern is that the facile solubility of both R6G and MG makes it spread in water sources and penetrate living organisms through the food chain [43]. Therefore, the influence of these dyes on human health has also been studied in many other works, thereby detecting the dyes, treating emitted residues, and making recommendations.

In this work, SiO_2@Ag nanocomposite was synthesized through the principles of the Stöber method with some modification technologies. As-synthesized SiO_2@Ag NCs would be investigated in terms of their optical and structural characteristics. At present, this SiO_2@Ag NC with multitasking can be used in MEF and SERS to detect organic dyes at dilute concentrations of MG and R6G.

Experimental

Tetraethoxysilane (TEOS) $Si(OC_2H_5)_4$ (99,98%), (3-aminopropyl) trimethoxysilane (APTMS) $H_2N(CH_2)_3Si(OCH_3)_3$ (99,96%), silver nitrate $AgNO_3$ (99,99%), sodium borohydride ($NaBH_4$), ammoniac NH_3 (25%), Rhodamine 6G (R6G), Malachite green (MG) (98%, solid, refractive index n = 1.5940, density $\rho = 1.0448$ g/cm^3, and molecular weight M = 364.911 g), absolute ethanol were purchased from Merck. All used chemicals were analytical grade. Deionized (DI) water was used in all experiments.

For fabricating SiO_2@Ag NCs, the process is illustrated in Scheme 1 with two steps. Firstly, SiO_2 particles were obtained according to the Stöber method [19] with slight modification. 5 ml of TEOS was dissolved in 30 ml of the ethanol and DI water solvent with a volume rate of 1:1, and then this solution was ultrasonicated for 15 min at room temperature to obtain an A solution. 3 ml of NH_3 was added into the A solution and stirred for 4 h to obtain a B mixture. The B mixture was centrifuged and filtered by absolute ethanol and DI water three times, then dried as precipitation at 80 °C for 15 h to obtain SiO_2 powder.

Secondly, 0.18 g of $AgNO_3$ was dissolved in 10 ml of DI water and 3 ml of NH_3 solution by magnetic stirring to make the C solution. Similarly, 0.01 g of $NaBH_4$ was dissolved in 10 ml of DI water to make the D solution. 0.2 g of as-synthesized SiO_2 was ultrasonicated with 50 ml ethanol for 15 min at room temperature to make an E solution. 0.1 ml of APTMS was added to the E solution and stirred for 15 h to produce the SiO_2-APTMS mixture (F). Then, the F mixture was centrifuged to obtain SiO_2-APTMS precipitations. The SiO_2-APTMS precipitations were added to the C solution and stirred for 2 h to make the G mixture. After that, the D solution was added to the G mixture and stirred for 15 min to obtain SiO_2@Ag precipitations. The precipitations were washed thrice with DI water and ethanol, then dried at 80 °C for 15 h to produce SiO_2@Ag NCs. The formation processes of the SiO_2@Ag nanocomposite are expressed in (1–5) as follows [2]:

$$Si(OC_2H_5)_4 + 2NH_4OH \rightarrow SiO_2 + 4C_2H_5OH + 2NH_3 \quad (1)$$

$$AgNO_3 + 3NH_4OH \rightarrow [Ag(NH_3)_2]OH + NH_4NO_3 + 2H_2O \quad (2)$$

$$SiO_2 + APTMS + [Ag(NH_3)_2]OH \rightarrow SiO_2 - APTMS@[Ag(NH_3)_2]OH \quad (3)$$

$$NaBH_4 + 4H_2O \rightarrow NaB(OH)_4 + 4H_2 \quad (4)$$

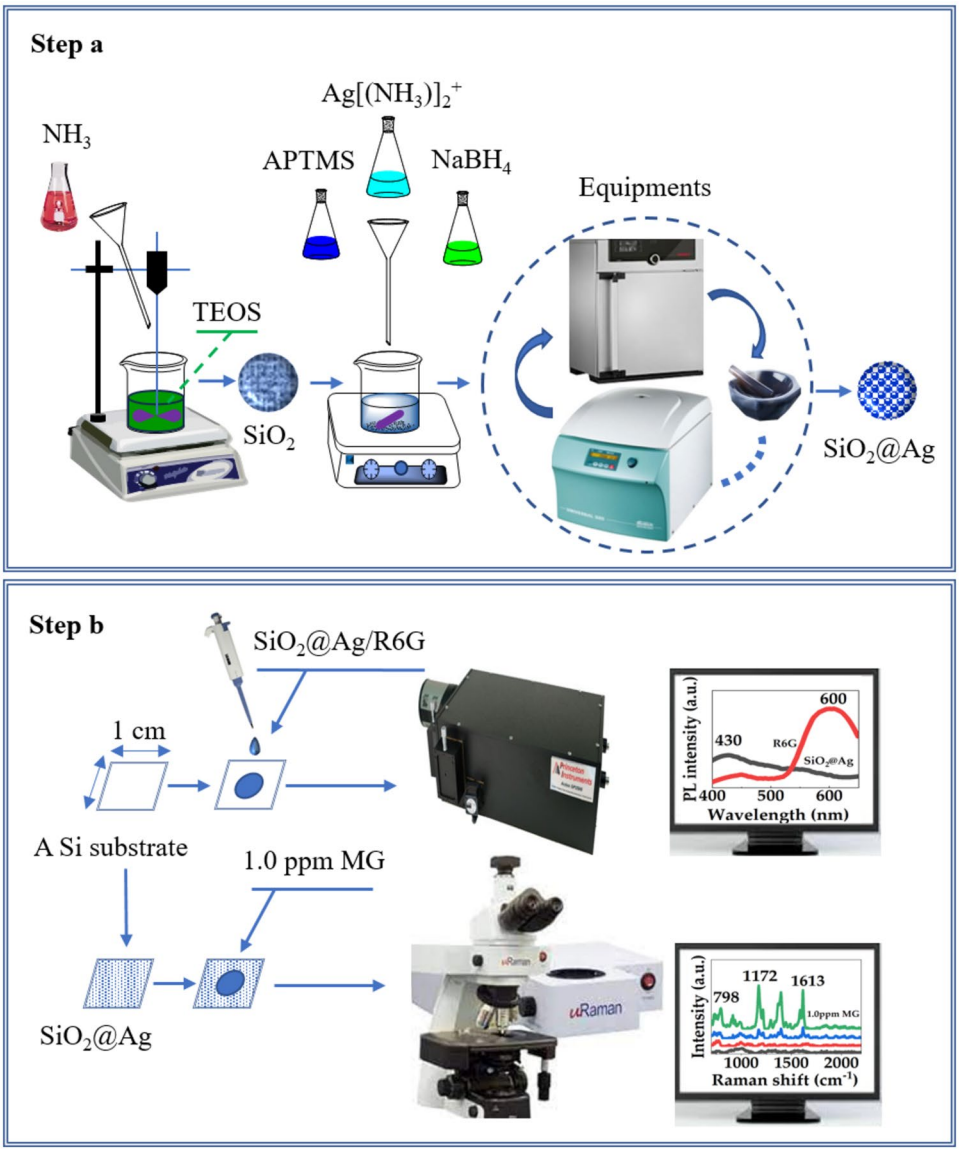

Scheme 1 The brief synthesis process of SiO_2@Ag and substrates preparation for MEF and SERS investigation

$$2[Ag(NH_3)_2]OH + 4NaB(OH)_4 + 6H_2O \rightarrow 2Ag^o + 15H_2 + 4H_3BO_3 + 4NaNO_3 \quad (5)$$

The synthesis process of SiO_2@Ag is presented briefly in Step a of the Scheme 1.

Thirdly, in order to investigate the MEF of SiO_2@Ag NCs for the R6G dye, SiO_2@Ag NCs and R6G were dispersed into DI water to make two different solutions at concentrations of 35.5 and 355 ppm, respectively. Two above solutions were mixed together to get solutions with the SiO_2@Ag to R6G volume ratio of (0:1), (1:1), (2:1), (3:1), (4:1), (5:1), (6:1), and (7:1), containing the R6G concentrations of 355, 177.5, 118.33, 88.75, 71, 59.17, 50.71, and 44.38 ppm, respectively. An equal amount of each solution was taken with a micropipette, deposited on the Si substrate, and let dry naturally. As-deposited Si substrates, samples, were denoted as R(0:1), R(1:1), R(2:1), R(3:1), R(4:1), R(5:1), R(6:1), and R(7:1) for MEF investigation.

Finally, with respect to preparations for the study of the SERS, the Si substrate with edge sizes of (1.0 cm × 1.0 cm) was cleaned in acetone, ethanol, and DI water, soaking in 50% HNO_3 for 15 min and in HF for 15 min. Let them dry naturally to get as-treated Si substrates. Then, a quantity of SiO_2@Ag solution with the 35.5 ppm concentration was deposited on the above as-treated Si substrates and dried to get SERS substrates. Afterwards, 10 µl of the 1.0 ppm MG solution was deposited on the SERS substrate area of 12.46 mm^2, drying to get the 1.0 ppm MG SERS substrate. MG with concentrations of 10^3 and 10^6 ppm were also deposited on Si substrate. As a result, there were four types of substrates: SiO_2@Ag, 10^3 ppm MG, and 10^6 ppm MG on Si substrates and 1.0 ppm MG on SERS substrate, which were

used for the SERS research, labelled as SiO_2@Ag, 10^3 ppm MG, 10^6 ppm MG, and 1.0 ppm MG, respectively. The preparation of substrates for the study of MEF and SERS is shown in Step b of the Scheme 1.

The microstructure and morphology of SiO_2 and SiO_2@Ag NC were investigated by X-ray diffraction (XRD) on a PANalytical Empyrean device using Cu_K_α radiation ($\lambda = 1.54056$ Å, $2\theta = 15^o$–70^o) and high-resolution transmission electron microscopy JEM-2100. The absorption spectra were recorded on the UV-2450 system. PL spectra were excited by the 325 nm radiation of the He-Cd laser on a Spectra Pro2500i system. Raman spectra were recorded on a portable μ Raman-Ci (Technospex) spectroscopy using a diode laser with technical specifications of power (10 mW), an excitation radiation (785 nm), a numerical aperture (NA = 0.5), and a laser spot area (2.9 μm^2). All spectra were recorded at room temperature.

Results and Discussions

Structure and Morphology of SiO_2@Ag Nanocomposite

The crystalline structure phase of SiO_2 and SiO_2@Ag NCs is shown by XRD patterns in Fig. 1. For the SiO_2, a broadband occurred at about 23.91° with weak intensity characterized by an amorphous structure phase. For the SiO_2@Ag NCs, the diffraction peaks at 37.94, 44.28, and 64.38° attributed to (111), (200), and (220) atomic planes of a face-centered cubic structure phase of Ag NPs, respectively, according to PDF N°: *96–901-3047*, which belongs to $Fm\bar{3}m$ space group. The diffraction peak of the (111) plane is narrow and most robust in the others; it is predicted that Ag particles achieve high crystallinity and big crystal sizes. While the characteristic band of the SiO_2 structure phase at 23.91° is weak, it further highlights the presence of Ag particles. From the XRD pattern, using Debye Scherrer and Bragg's formulas [3, 4, 16], the average particle size and lattice d-spacing of Ag NPs are calculated at about 24 nm and 2.38 Å, respectively. The characteristic peaks for the silver structural phase in the XRD pattern of SiO_2@Ag NCs showed that Ag NPs had been formed on the SiO_2 surface [21]. For easy visualization, the mechanism of Ag NP decorated on SiO_2 NSs is described as follows: the F solution is a SiO_2-APTMS colloidal system containing negative NH_2-amin groups. When adding the $Ag[(NH_3)]_2^+$ ion solution to the F, Ag^+ ions have been absorbed on the SiO_2 surface due to the interaction between NH_2- groups and $Ag(NH_3)^+$ ions to form the G mixture (SiO_2-APTMS-$Ag[(NH_3)]_2^+$. Therefore, after the $NaBH_4$ solution was added, Ag^+ ions on the surface of SiO_2 NSs were reduced to Ag NPs. Those are illustrated in Fig. 2 [44]. The structural phase, shape, and size of the SiO_2@Ag NCs are shown in Fig. 3. The TEM image showed

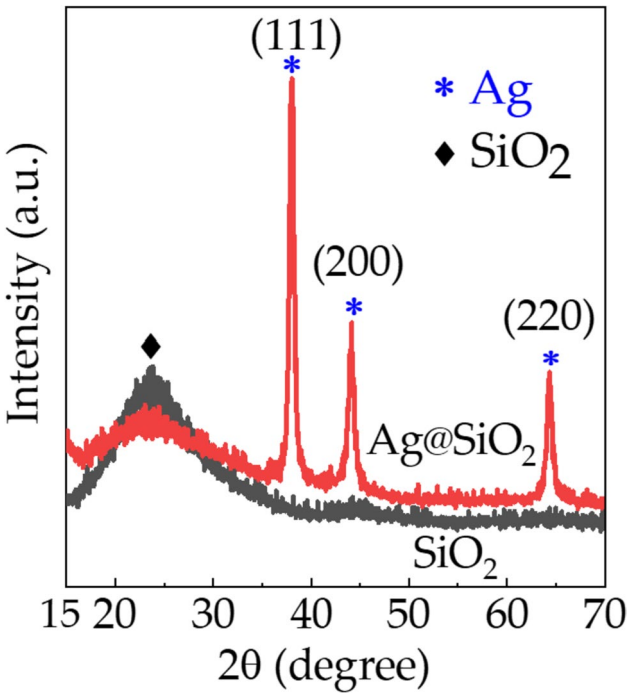

Fig. 1 XRD patterns of SiO_2 and SiO_2@Ag NCs

that SiO_2 particles possessed spherical shape with sizes in the range of 100–180 nm (Fig. 3a), but the distributed SiO_2 NSs concentrated at an average size of 132 nm (Fig. 3c). The inset showed that the Ag NPs on SiO_2 spheres were not agglomerated. HR-TEM image is observed that the lattice ridges are oriented in the same parallel direction representing a single grain (Fig. 3c). The d-spacing between two consecutive (111) planes was determined about 2.4 Å (the inset of Fig. 3c) likely an estimated result by the XRD pattern [13]. It also confirmed that Ag NPs were decorated on the SiO_2 NSs. The SAED pattern of Ag NP consists of bright spots representing the crystal structure phase (Fig. 3d) [5]. Basically, the bright spots are located on the concentric circle fringes, in which three fringes correspond to the (111), (200), and (220) planes in the XRD pattern [9].

The MEF and SERS Properties of SiO_2@Ag Nanocomposites

Figure 4 presents the UV–Vis absorption spectrum (a) of SiO_2@Ag NCs and R6G solutions and PL spectra (b) of SiO_2@Ag NCs and R6G solutions deposited on Si substrate with the concentration of 35.5 and 355 ppm (R(1:0), R(0:1)), respectively. The Gaussian symmetry of the UV–Vis absorption spectrum of SiO_2@Ag evidenced that Ag NPs have a quasi-spherical shape with a concentrated size distribution [16]. The maximum position of that absorption spectrum is centered at about 400 nm, derived from the SPR of Ag NPs

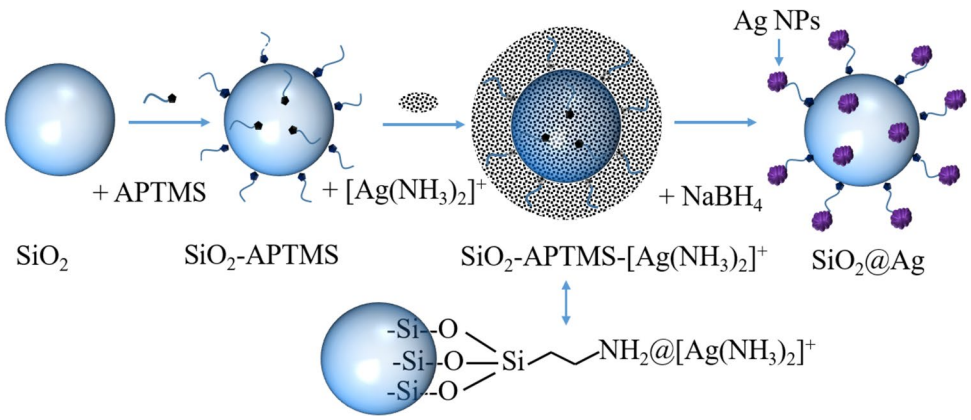

Fig. 2 Mechanism of as-decorated Ag NPs on SiO_2 surface

(Fig. 4a) [14]. The SPR spectrum is only recorded on the metal surface, proving that the reduced Ag NPs are attached to the SiO_2 surface. There are several factors responsible for the enhancement. The first is the effect of local field enhancement generated near metallic structures [45, 46]. Another factor is the plasmon-coupling effect mediated by a non-radiative interaction [47]. If the plasmonic structure and the fluorophore are at an optimal distance, the energy transfer between them is dominated. Those are explained by Förster (or fluorescence) resonance energy transfer, the mechanism of electron transfer through molecules. The non-radiative energy transfer between metal and fluorophore depends not only on the strength of the electric field but also on the degree of spectral overlap between the metal surface and the fluorophore [46]. A broad 525 nm absorption band appeared in the UV- Vis absorption spectrum of R6G (Fig. 4a). There is quite a good overlap between the absorption of R6G and SiO_2@Ag.

Therefore, R6G is used to study the ability of fluorescence enhancement of SiO_2@Ag NCs. In the R6G molecular structure, there are π-bonds of C = C, C = N, and C = O groups, as seen in the inset of Fig. 4a. The optical properties

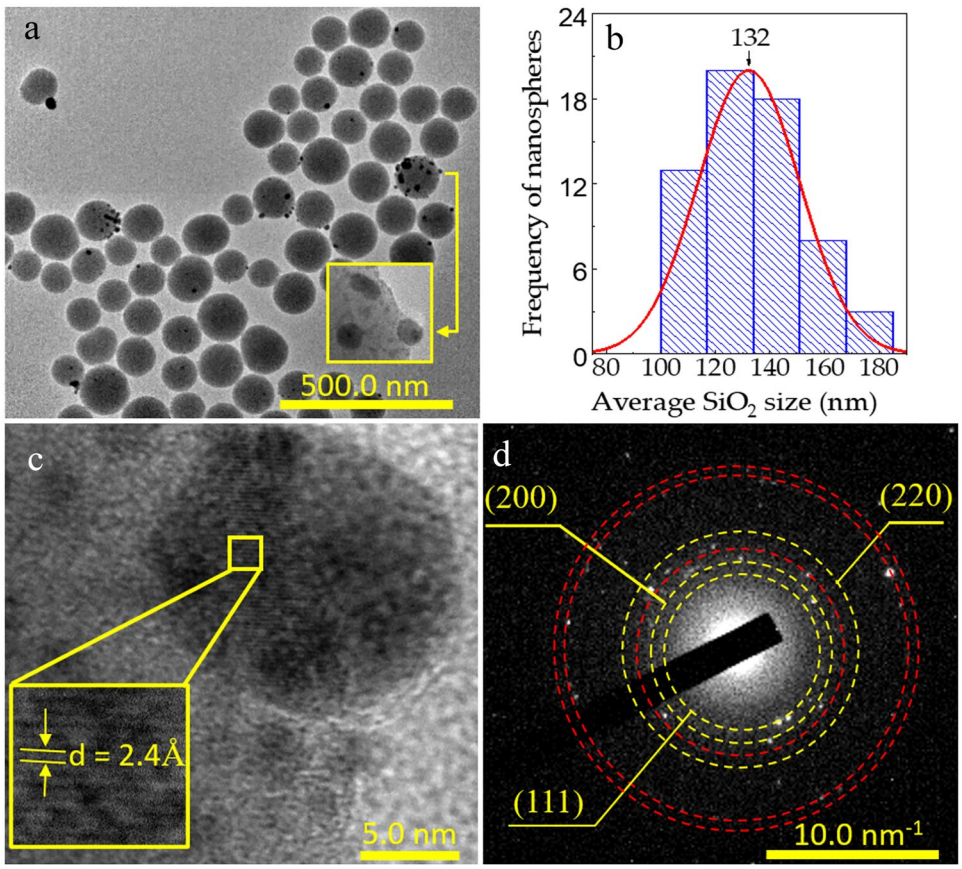

Fig. 3 **a** TEM image, **b** particle distribution histogram, **c** HR-TEM image, and **d** SAED pattern of SiO_2@Ag NCs

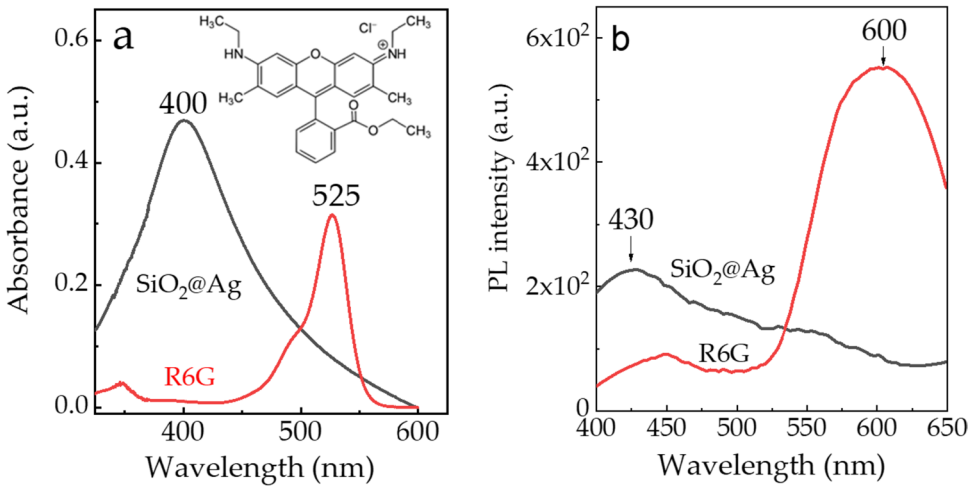

Fig. 4 **a** UV–Vis absorption spectra of SiO_2@Ag NCs and R6G solutions and inserted figure as R6G molecule, and **b** PL spectra of SiO_2@Ag NCs and R6G on Si substrates

of the R6G are related to the electronic transitions between π and π* orbital states [48]. As observed in the PL spectrum of SiO_2@Ag in Fig. 4b, the broadband at about 430 nm originated from different defect centers of SiO_2 NSs [49, 50]. The PL spectrum of the R6G appears to be a band at 600 nm. However, it is robust in comparison with SiO_2@Ag in terms of the PL intensity. This band is caused by the emission of dimers [23–26], but the nature is still related to the electric transitions from $S_1(\pi^*)$ excited state to $S_o(n, \pi)$ ground state [48]. Furthermore, the R6G concentration of 355 ppm seems quite dense, as the PL maximum peak is located at 600 nm, belonging to the sort of dimer [23].

Notably, there is a strong enhancement in both MEF and SERS using SiO_2@Ag NCs. Figure 5 manifests the PL spectra of the R6G with different volume ratios between SiO_2@Ag and R6G, in which the PL spectrum of R6G is redrawn. All PL spectra show a band with a maximum in the range of 553–560 nm but not at 600 nm, as explained in Fig. 4b. The shape of PL spectra is asymmetric, left-steep, and right-gentle due to the overlap of dimer-monomer PL bands, herein, the monomer band is more dominant than the dimer one [27, 51]. In the case of a SiO_2@Ag NCs absence, the PL spectrum of the R6G (R(0:1)) appears extremely weak, resembling a baseline. However, using SiO_2@Ag NCs, the PL intensity of the R6G becomes much stronger, and the peak position of the PL band depends on the change of the SiO_2@Ag to R6G volume ratio. In order to estimate the EF_{MEF}, a compared calculation between the absolute PL intensity of the R6G at R(5:1) and the one at R(0:1) was expressed as [28, 29]:

$$EF_{MEF} = \left(I_{R(5:1)} - I_{SiO_2@Ag}\right).\left(I_{R(0:1)} - I_{SiO_2@Ag}\right)^{-1} \quad (6)$$

In Eq. (6), $I_{R(5:1)}$, $I_{(R(0:1))}$, and $I_{SiO_2@Ag}$ are absolute intensities according to the SiO_2@Ag to R6G volume ratios and SiO_2@Ag substrate. Note that the spectral signal from the Si substrate was feeble in the observed region under the excitation radiation of 325 nm; it was not mentioned. When the volume ratio is R(1:1), the absolute PL intensity of the 560 nm band is 24 times as much as that of the 600 nm band

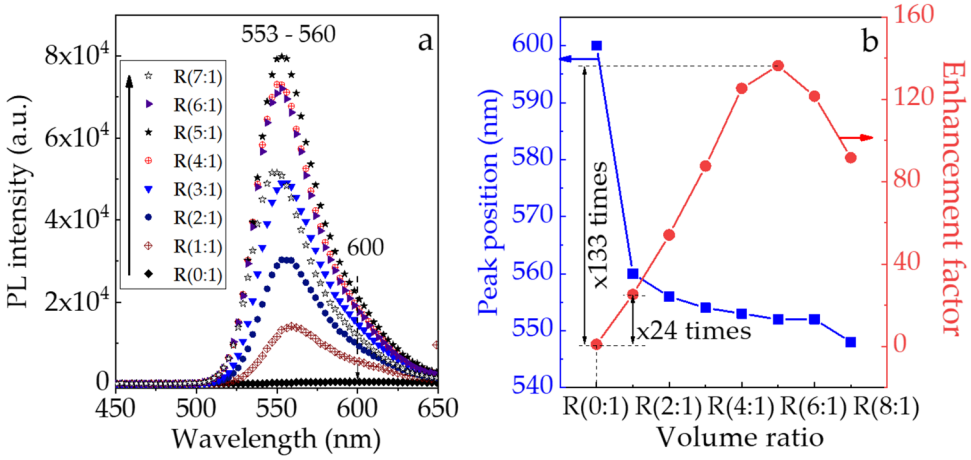

Fig. 5 **a** PL spectra of R6G using SiO_2@Ag NCs, and **b** Peak position and enhancement factor versus SiO_2@Ag to R6G volume ratios

of R(0:1). From R(2:1) to R(4:1), the PL intensity also goes up while the maximum position shifts towards to the shorter wavelength. At the volume ratio of R(5:1), the PL intensity reaches the maximum and rises by 133 times in comparison with the intensity of R(0:1). Afterwards, the PL intensity decreases despite increasing the volume ratio from R(6:1) to R(7:1). The maximum position and EF_{MEF} as functions of volume ratios are delineated in Fig. 5b. The change in optical R6G spectra according to the SiO_2@Ag to R6G volume ratio can be explained, based on the distance change between R6G and Ag NPs. It is known that a suitable distance between R6G and Ag NPs will exist for the best energy transfer process so that the PL intensity is the strongest. Yet the PL intensity will be quenched if the formed distance differs from the above suitable one [25, 52]. In the case of R(5:1), about 59.17 ppm of the R6G, the distance between R6G and Ag NPs can be the most suitable for the energy transfer, increasing the PL [25]. In addition, it can also be due to the change of SiO_2@Ag to R6G volume ratio, as the R6G concentration is changed, leading to the change of the energy transfer distance [53]. The energy transfer process between coated polymers and nanoparticles of composite materials has also been known [54, 55]. It can be seen that, herein, the surface-functionalized SiO_2 spheres possessed the functional -NH_2 groups of APTMS molecules as anchors attracting both Ag NPs and R6G molecules on the surface of the SiO_2 NSs, so there always ensured a suitable distance between them for the MEF effect. Therefore, Ag NPs decorated SiO_2 NSs also have a good MEF in comparison with Ag NPs [29–31, 33], coated Ag NPs [28, 32], core–shell Ag@SiO_2 structures [22, 34], and Ag multilayers [35], as shown in Table 1.

As-synthesized SiO_2@Ag NCs have not only the ability of MEF but also SERS. Figure 6 presents Raman spectra of SiO_2@Ag, 10^3, 10^6, and 1.0 ppm MG on different substrates. In the case of SERS (at 1.0 ppm MG), a series of peaks appear clearly at 798, 916, 1172, 1365, 1394, and 1613 cm^{-1}, which are attributed to vibrations, respectively, ring C–H out-of-plane bending (798 and 916 cm^{-1}), ring C–H in-plane bending (1172 cm^{-1}), N-phenyl stretching (1365 cm^{-1}), C-N symmetrical stretching (1394 cm^{-1}), and ring C–C stretching (1613 cm^{-1}) [36, 56]. While the Raman signals of SiO_2@Ag and 10^3 ppm MG are recorded too weak, peaks are not shown obviously in Fig. 6a. It is affirmed that the peaks at 798, 916, 1172, 1365, 1394, and 1613 cm^{-1} do not belong to the SiO_2@Ag and Si substrates. The SERS was not caused by the Si substrate, even though the MG concentration was utilized to be 10^3 ppm [57], or owing to the characteristic peak of the Si substrate in different wavenumber regions [58]. Only if the MG concentration is equal to 10^6 ppm, a series of peaks at 1172, 1394, and 1613 cm^{-1} are observed in the normal Raman spectrum. As seen in the 1172 cm^{-1} mode in Fig. 6b, the intensity of the SERS signal is stronger than that of the normal Raman signal; this is also true for the others. The cause of the SERS is due to the resonance of the vibrational modes with the electromagnetic field at the hot spots, as mentioned above. To evaluate the enhancement factor of the SERS intensity on

Table 1 Comparison of EF_{MEF} and EF_{SERS} values of various materials for organic compounds

Materials	Organic compounds	EF_{MEF}	EF_{SERS}	References
Ag@SiO_2@RITC@SiO_2	Rhodamine B isothiocyanate	5	-	[22]
SiO_2-Ag-cicada wing	R6G	1.99	-	[28]
Flowerlike silver nanostructures	R6G	71	-	[29]
Silver nanostructures	SH-oligomer-Cyanine 5	25	-	[30]
Silver islands films	Rhodamine B	6	-	[31]
Ag@SiO_2 NCs	Glucose	4.9	-	[32]
Silver NPs	Fluorescein, Cyanine 3, and Cyanine 5	10–20	-	[33]
Ag@SiO_2 NCs	Rhodamine 800	20	-	[34]
Silver-SiO_2-Silver Nanoburger	Fluorescein isothiocyanate	35		[35]
SiO_2@Ag NCs	R6G	133	-	This work
Starch-coated Ag NPs	MG	-	5.11×10^5	[38]
Ag decorated microstructured PDMS	MG	-	2.06×10^5	[39]
Ag NPs	MG	-	7.9×10^6	[40]
Ag NPs modified glass fiber paper	MG	-	1.3×10^8	[41]
Ag NPs	MG	-	1.5×10^5	[42]
SiO_2@Ag NCs	MG	-	6.3×10^6	This work

- Nonivestigation

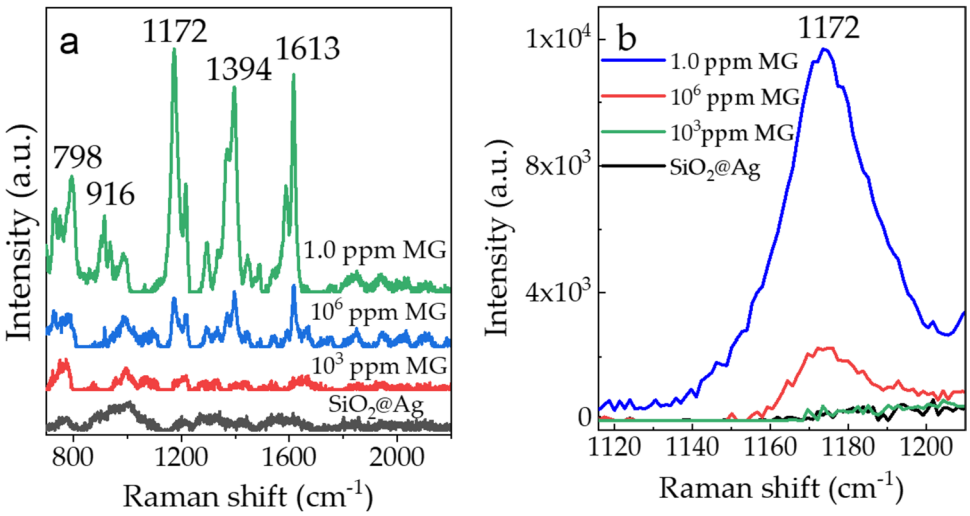

Fig. 6 **a** Raman spectra of SiO_2@Ag, 10^3, and 10^6 ppm MG deposited on Si substrate and 1.0 ppm MG deposited on SERS substrate and **b** A region of enlarged Raman spectra for 1172 cm^{-1} peak

the SiO_2@Ag substrate in comparison with normal Raman intensity on the Si substrate, the EF_{SERS} can be determined by the following formula (7) [59]:

$$EF_{SERS} = \left(I_{SERS}.C_{Raman}\right)/\left(I_{Raman}.C_{SERS}\right) \quad (7)$$

where I_{SERS} and I_{Raman} are the integrated intensities of the SERS and the normal Raman spectrum, respectively. C_{SERS} and C_{Raman} are the concentrations of MG solutions deposited on the SiO_2@Ag substrate for SERS analysis and the Si substrate for normal Raman analysis. Note that the diode laser worked under the same experimental conditions for all SERS and normal Raman analyses. Used MG volume and MG-covered surface area on both substrates are 10 µl and 12.46 mm^2, respectively, as presented in experiments. Consider that SiO_2@Ag NCs and MG molecules are distributed uniformly on the surface of Si substrates. Thus, the C_{SERS} and C_{Raman} equal 1.0 and 10^6 ppm, respectively. For the 1172 cm^{-1} peaks, by integrating the intensity, the EF_{SERS} was estimated to be approximately 6.3×10^6. The calculated EF_{SERS} value is sensitive to 1.0 ppm MG and close to the other results in Table 1 [38–42].

Thus, it can be concluded that the as-fabricated SiO_2@Ag NCs have the capabilities for MEF and SERS. Ag NPs were glued to the spherical SiO_2 surface by APTMS molecules via the reduction process, so Ag NPs are fixed on the surface of SiO_2 NSs. Consequently, hot spots were also created where the dye molecules were located at a suitable distance to enhance fluorescence and Raman scattering signals. The PL intensity of the R6G increased strongly when the SiO_2@Ag content was small at the R(1:1). It reached maximum and was observed easily at the R(5:1) with the R6G concentration of 59.17 ppm. Besides, the SERS signal is obtained so strongly for probing MG dye at the concentration of 1.0 ppm.

Conclusion

In summary, we have demonstrated a facile way to synthesize SiO_2@Ag nanocomposite based on Stöber's method and a chemical reduction process. As-formed Ag nanoparticles in quasi-spherical shapes with an average crystallite size of 24 nm were decorated on the SiO_2 surfaces. The decoration of the Ag nanoparticle is necessary to create a suitable distance for the energy transfer between the dye and the Ag nanoparticle. The PL intensity increased by 133 times at the SiO_2@Ag to R6G volume ratio of (5:1) for probing the R6G at 59.17 ppm. The SERS enhancement factor reached approximately 6.3×10^6 to detect the MG concentration at 1.0 ppm.

Acknowledgements This research has been done under the project QG.22.15 of Vietnam National University, Hanoi.

Author Contributions All authors contributed to the study conception and design. Material preparation, data collection and analysis were performed by Dang Van Thai, Van Ben Pham, Cong Doanh Sai, Thi Huong Giang Nguyen, Trong Duc Tran, Thi Ha Tran, Tien-Thanh Nguyen, Tien Dai Nguyen, and Hong Van Bui. The first draft of the manuscript was written by Dang Van Thai and Hong Van Bui, and all authors commented on previous versions of the manuscript. All authors read and approved the final manuscript.

Funding The funder has been acknowledged in the acknowledgment section. Author Hong Van Bui has received research support from the Vietnam National University.

Data Availability The data for this work will be made available on request.

Declarations

Ethical Approval Not applicable.

Competing Interests The authors declare no competing interests.

References

1. Chatterjee K, Sarkar S (2014) Core/shell nanoparticles in biomedical applications. Adv Coll Interface Sci 209:8–39. https://doi.org/10.1016/j.cis.2013.12.008
2. Malekzadeh M, Yeung KL, Halali M, Chang Q (2019) Preparation and antibacterial behaviour of nanostructured Ag@SiO_2 penicillin with silver nanoplates. New J Chem 43:16612–16620. https://doi.org/10.1039/c9nj03727f
3. Rodrigues MC, Rolimc WR, Viana MM, Souza TR, Gonçalves F, Tanaka CJ, Bueno-Silva B, Seabra AB (2020) Biogenic synthesis and antimicrobial activity of silica-coated silver nanoparticles for esthetic dental applications. J Dent 96:103327. https://doi.org/10.1016/j.jdent.2020.103327
4. Al-Bermany E, Mekhalif ATM, Banimuslem HA, Abdali K, Sabri MM (2023) Effect of green synthesis bimetallic Ag@SiO2 core-shell nanoparticles on absorption behavior and electrical properties of PVA-PEO nanocomposites for optoelectronic applications. Silicon 15:4095–4107. https://doi.org/10.1007/s12633-023-02332-7
5. Sakthisabarimoorthi A, Jose M, Martin Britto Dhas SA, Jerome Das S (2017) Fabrication of Cu@Ag core-shell nanoparticles for nonlinear optical applications. J Mater Sci: Mater Electron 28:4545–4552. https://doi.org/10.1007/s10854-016-6090-0
6. Kim YH, Lee DK, Cha HG, Kim CW, Kang YS (2007) Synthesis and characterization of antibacterial Ag-SiO_2 nanocomposite. J Phys Chem C 111:3629–3635. https://doi.org/10.1021/jp068302w
7. Peters RJ, Bouwmeester H (2016) Nanomaterials for products and application in agriculture, feed and food. Trends Food Sci Technol 54:155–164. https://doi.org/10.1016/j.tifs.2016.06.008
8. Karthik C, Caroline DG, Dhanam Priya M, Pandi Prabha S (2021) Synthesis, characterization of Ag-SiO_2 nanocomposite and its application in food packaging. J Inorg Organometall Polym Mater 31:2532–2541. https://doi.org/10.1007/s10904-020-01853-7
9. Zhang Y, Sun H, Gao R, Zhang F, Zhu A, Chen L, Wang Y (2018) Facile SERS-active chip (PS@Ag/SiO_2/Ag) for the determination of HCC biomarker. Sens Actuators, B Chem 272:34–42. https://doi.org/10.1016/j.snb.2018.05.139
10. Assis M, Luiz GP, Simoes GC, Tremiliosi LK, Ribeiro DC, Minozzi DT, Santos RI, Vilela DCB, Mascaro LH, Andrés J, Longo E (2021) PVC-SiO 2-Ag composite as a powerful biocide and anti-SARS-CoV-2 material. J Polym Res 28:361. https://doi.org/10.1007/s10965-021-02729-1
11. Alimunnisa J, Ravichandran K, Meena KS (2017) Synthesis and charactirization of Ag@SiO_2 core-shell nanoparticles for antibacterial and environmental applications. J Mol Liq 231:281–287. https://doi.org/10.1016/j.molliq.2017.01.103
12. Feng X, Li H, Zhang Q, Zhang P, Song X, Liu J, Zhao L, Gao L (2016) SiO_2-Ag-SiO_2 core/shell structure with a high density of Ag nanoparticles for CO oxidation catalysis. Nanotechnology 27:455605. https://doi.org/10.1088/0957-4484/27/45/455605
13. Khedkar CV, Daware KD, Badgujar PS, Kolekar YD, Gosavi SW, Patil SI (2021) Ag-SiO_2 nanocomposite for the optical detection of Hg(II) ions and catalytic reduction of methylene blue. Opt Mater 120:111426. https://doi.org/10.1016/j.optmat.2021.111426
14. Alimunnisa J, Zhi Gang Wu, Jia YR, Wang J, Gui Y, Gao JF (2016) Core-shell SiO_2/Ag composite spheres: synthesis, characterization and photocatalytic properties. Mater Sci-Pol 34:806–810. https://doi.org/10.1515/msp-2016-0121
15. Etchegoin PG, Le Ru EC (2008) A perspective on single molecule SERS: current status and future challenges. Phys Chem Chem Phys 10:6079–6089. https://doi.org/10.1039/B809196J
16. Taib T, Johan MR, Basirun WJ (2021) Plasmonic SERS active nanostructured Ag-SiO_2 at optimum volume ratio synthesized via sol-gel technique. Physica B: Phys Condens Matter 606:12638. https://doi.org/10.1016/j.physb.2020.412638
17. Cheshari EC, Ren X, Li X (2019) Core-shell Ag molecularly imprinted composite for SERS detection of carbendazim. Int J Environ Anal Chem 100:1245–1258. https://doi.org/10.1080/03067319.2019.1651301
18. Ahemad MJ, Yeon-Tae Yu (2020) Investigating the mechanism of uniform Ag@SiO_2 core-shell nanostructures synthesis by a one-pot sol-gel method. J Sol-Gel Sci Technol 96:679–689. https://doi.org/10.1007/s10971-020-05392-y
19. Stöber W, Fink A, Bohn E (1968) Controlled growth of monodisperse silica spheres in the micron size range. J Colloid Interface Sci 26:62–69. https://doi.org/10.1016/0021-9797(68)90272-5
20. Mock JJ, Barbic M, Smith DR, Schultz DA, Schultz S (2002) Shape effects in plasmon resonance of individual colloidal silver nanoparticles. J Chem Phys 116:6755–6759. https://doi.org/10.1063/1.1462610
21. Huang J, Zhou Y-F, Jian Xu, Liang P, Liu Z-G, Wang J, Zhang De, Dong Q-M, Shen W-M, Zhuang S-L (2019) Unveiling the growth mechanism of SiO_2/Ag hybrid nanospheres and using for Surface Enhanced Raman Scattering detection. Appl Surf Sci 463:115–120. https://doi.org/10.1016/j.apsusc.2018.08.220
22. Gua L, Guan A, Lin X, Zhang C, Chen G (2010) Preparation of a new core-shell Ag@SiO_2 nanocomposite and its application for fluorescence enhancement. Talanta 82:1696–1700. https://doi.org/10.1016/j.talanta.2010.07.051
23. Zehentbauer FM, Moretto C, Stephen R, Thevar T, Gilchrist JR, Pokrajac D, Richard KL, Kiefer J (2014) Fluorescence spectroscopy of Rhodamine 6G: Concentration and solvent effects. Spectrochim Acta Part A Mol Biomol Spectrosc 121:147–151. https://doi.org/10.1016/j.saa.2013.10.062
24. Purcar V, Donescu D, Petcu C, Vasilescu M (2008) Nanostructured hybrid systems with rhodamine 6G. J Dispersion Sci Technol 29:1233–1239. https://doi.org/10.1080/01932690701856915
25. Zhao J, Jensen L, Sung J, Zou S, Schatz GC, Van Duyne RP (2007) Interaction of Plasmon and Molecular Resonances for Rhodamine 6G Adsorbed on Silver Nanoparticles. J Am Chem Soc 129:7647–7656. https://doi.org/10.1021/ja0707106
26. Sasai R, Iyi N, Fujita T, Arbeloa FL, Martínez Takagi K, Itoh H (2004) Luminescence properties of rhodamine 6G intercalated in surfactant/clay hybrid thin solid films. Langmuir 20:4715–4719. https://doi.org/10.1021/la049584z
27. Yeshchenko OA, Bondarchuk IS, Kozachenko VV, Losytskyy MY (2015) Photoluminescence of rhodamine 6G in plasmonic field of Au nanoparticles: Temperature effects. J Lumin 158:294–300. https://doi.org/10.1016/j.jlumin.2014.10.018
28. Pan S, Zhu Y, Shi G, Shang Z, Wang M (2020) Synthesis of SiO_2 coated Ag-cicada wing as large scale surface enhanced fluorescence substrate. Optik - Int J Light Electr Opt 223:165377. https://doi.org/10.1016/j.ijleo.2020.165377
29. Zhang Y, Yang C, Zhang G, Peng Z, Yao L, Wang Q, Cao Z, Mu Q, Xuan L (2017) Distance-dependent metal enhanced fluorescence by flowerlike silver nanostructures fabricated in liquid crystalline phase. Opt Mater 72:289–294. https://doi.org/10.1016/j.optmat.2017.06.020
30. Li H, Chen C-Y, Wei X, Qiang W, Li Z, Cheng Q, Xu D (2012) Highly sensitive detection of proteins based on metal enhanced fluorescence with novel silver nanostructures. Anal Chem 84:8656–8662. https://doi.org/10.1021/ac301787x
31. Ray K, Badugu R, Lakowicz JR (2007) Polyelectrolyte Layer-by-Layer Assembly To Control the Distance between Fluorophores and Plasmonic Nanostructures. Chem Mater 19:5902–5909. https://doi.org/10.1021/cm071510w
32. Jang E, Kim M, Koh W-G (2015) Ag@SiO_2-entrapped hydrogel microarray: a new platform for a metal-enhanced

fluorescence-based protein assay. Analyst 140:3375–3383. https://doi.org/10.1039/C5AN00251F
33. Corrigan TD, Guo S, Phaneuf RJ, Szmacinski H (2005) Enhanced fluorescence from periodic arrays of silver nanoparticles. J Fluoresc 15:777–784. https://doi.org/10.1007/s10895-005-2987-3
34. Aslan K, Meng Wu, Lakowicz JR, Gedde CD (2007) Metal enhanced fluorescence solution-based sensing platform 2: Fluorescent core-shell Ag@SiO_2 nanoballs. J Fluoresc 17:127–131. https://doi.org/10.1007/s10895-007-0164-6
35. Zhang Y, Mandeng LN, Bondre N, Dragan A, Geddes CD (2010) Metal-enhanced fluorescence from silver-SiO_2-silver nanoburger structures. Langmuir 26:12371–12376. https://doi.org/10.1021/la101801n
36. Zhang Y, Wansong Yu, Pei Lu, Lai K, Rasco BA, Huang Y (2015) Rapid analysis of malachite green and leucomalachite green in fish muscles with surface-enhanced resonance Raman scattering. Food Chem 169:80–84. https://doi.org/10.1016/j.foodchem.2014.07.129
37. Zhao Y, Tian Y, Ma P, Aimin Yu, Zhang H, Chen Y (2015) Determination of melamine and malachite green by surface-enhanced Raman scattering spectroscopy using starch-coated silver nanoparticles as substrates. Anal Methods 7:8116–8122. https://doi.org/10.1039/c5ay01540e
38. Jiang J, Shen Q, Xue P, Qi H, Yunpeng Wu, Teng Y, Zhang Y, Liu Y, Zhao X, Liu X (2020) A highly sensitive and stable SERS sensor for malachite green detection based on Ag nanoparticles in situ generated on 3D MoS_2 nanoflowers. ChemistrySelect 5:354–359. https://doi.org/10.1002/slct.201903924
39. Kumar P, Khosla R, Soni M, Deva D, Sharma SK (2017) A highly sensitive, flexible SERS sensor for malachite green detection based on Ag decorated microstructured PDMS substrate fabricated from Taro leaf as template. Sens Actuators B Chem 246:477–486. https://doi.org/10.1016/j.snb.2017.01.202
40. Ouyang L, Yao L, Zhou T, Zhu L (2018) Accurate SERS detection of malachite green in aquatic products on basis of graphene wrapped flexible sensor. Anal Chim Acta 16:83–91. https://doi.org/10.1016/j.aca.2018.04.052
41. Deng Di, Lin Q, Li H, Huang Z, Kuang Y, Chen H, Kong J (2019) Rapid detection of malachite green residues in fish using a surface-enhanced Raman scattering-active glass fiber paper prepared by in situ reduction method. Talanta 200:272–278. https://doi.org/10.1016/j.talanta.2019.03.021
42. Polavarapu L, La Porta A, Novikov SM, Coronado-Puchau M, Liz-Marzán LM (2014) Pen-on-paper approach toward the design of universal surface enhanced raman scattering substrates. Small 10:3065–3071. https://doi.org/10.1002/smll.201400438
43. Srivastava S, Sinha R, Roy D (2004) Toxicological effects of malachite green. Aquat Toxicol 66:319–329. https://doi.org/10.1016/j.aquatox.2003.09.008
44. Zeng R, Liu L, Li S, ZouZhang YF, Yang Y, Cui H, Han EH (2013) Self-assembled silane film and silver nanoparticles coating on magnesium alloys for corrosion resistance and antibacterial applications. Acta Metallurgica Sinica (English Letter) 26:681–686. https://doi.org/10.1007/s40195-013-0397-0
45. Scott ML, Cushing K, Nianqiang Wu (2015) Plasmon-enhanced optical sensors: a review. Analyst 140(2):386–406. https://doi.org/10.1039/C4AN01079E
46. Lakowicz JR, Ray K, Chowdhury M, Szmacinski H, Yi Fu, Zhang J, Nowaczyk K (2008) Plasmon-controlled fluorescence: a new paradigm in fluorescence spectroscopy. Analyst 133(10):1308–1346. https://doi.org/10.1039/B802918K
47. Aslan K, Leonenko Z, Lakowicz JR, Geddes CD (2005) Annealed silver-island films for applications in metal-enhanced fluorescence: interpretation in terms of radiating plasmons. J Fluoresc 15(5):643. https://doi.org/10.1007/s10895-005-2970-z
48. Aydemir M, Jankus V, Dias FB, Monkman A (2014) The key role of geminate electron-hole pair recombination on delayed fluorescence in Rhodamine 6G and ATTO-532. Phys Chem Chem Phys 16:21543–21549. https://doi.org/10.1039/C4CP01675K
49. Mbakaan C, Ahemen I, Amah AN, Onojah AD, Koao L (2018) White-light-emitting Dy^{3+}-doped amorphous SiO_2 nanophosphors derived from rice husk. Appl Phys A 124:741. https://doi.org/10.1007/s00339-018-2156-6
50. Uma K, Chen S-W, KrishnaKumar B, Jeyaprabha C, Yang T-K, Lin J-H (2021) Enhanced photocatalytic activity of CdS nanostar decorated SiO_2/TiO_2 composite spheres and the simulation effect using FDTD model. Ionics 27:397–406. https://doi.org/10.1007/s11581-020-03795-z
51. Landau A, Zaban A, Lapides I, Yariv S (2002) Montmorillonite treated with rhodamine-6G mechanochemically and in aqueous suspensions simultaneous Dta-Tg study. J Therm Anal Calorim 70:103–113. https://doi.org/10.1023/A:1020649416016
52. Jeong Y, Kook Y-M, Lee K, Koh W-G (2018) Metal enhanced fluorescence (MEF) for biosensors: General approaches and a review of recent developments. Biosens Bioelectron 111:102–116. https://doi.org/10.1016/j.bios.2018.04.007
53. Basheer NS, Kumar BR, Kurian A, George SD (2013) Thermal lens probing of distant dependent fluorescence quenching of Rhodamine 6G by silver nanoparticles. J Lumin 137:225–229. https://doi.org/10.1016/j.jlumin.2012.12.052
54. Van Thai D, Van Ben P, Trung VQ, Van BH, Nghia NM, Thi TM (2023) Luminescence enhancement of ZnS: Mn and ZnS:Cu-PVP nanoparticles by laser radiation annealing. Opt Mater 135:113020. https://doi.org/10.1016/j.optmat.2022.113020
55. Van Thai D, Van Ben P, Thi TM, Van Truong N, Thu HH (2016) The photoluminescence enhancement of Mn^{2+} ions and the crystal field in ZnS: Mn nanoparticles covered by polyvinyl alcohol. Opt Quant Electron 48:362. https://doi.org/10.1007/s11082-016-0622-y
56. Zhang Y, Huang Y, Kang Y, Miao J, Lai K (2021) Selective recognition and determination of malachite green in fish muscles via surface-enhanced Raman scattering coupled with molecularly imprinted polymers. Food Control 130:108367. https://doi.org/10.1016/j.foodcont.2021.108367
57. Bontempi N, Vassalini I, Danesi S, Ferroni M, Donarelli M, Colombi P, Alessandri I (2018) Non-plasmonic SERS with silicon: Is it really safe? New insights into the opto-thermal properties of core/shell microbeads. J Phys Chem Lett 9:2127–2132. https://doi.org/10.1021/acs.jpclett.8b00662
58. Kamyczek P, Placzek-Popko E, Zytkiewicz ZR, Gumienny Z, Zielony E, Sobanska M, Klosek K, Reszka A (2013) Structural and optical characterization of GaN nanowires. J Appl Phys 113:204303. https://doi.org/10.1063/1.4808097
59. Le Ru EC, Blackie E, Meyer M, Etchegoin PG (2007) Surface enhanced raman scattering enhancement factors: a comprehensive study. J Phys Chem C 111:13794–13803. https://doi.org/10.1021/jp0687908